energies

MDPI

Review

Photoemission Studies on the Environmental Stability of Thermal Evaporated $MAPbI_3$ Thin Films and $MAPbBr_3$ Single Crystals

Ke Wang, Benjamin Ecker and Yongli Gao *

Department of Physics and Astronomy, University of Rochester, Rochester, NY 14627, USA; kwang41@ur.rochester.edu (K.W.); becker@ur.rochester.edu (B.E.)
* Correspondence: ygao@pas.rochester.edu

Abstract: Hybrid organic inorganic perovskites have been considered as a potential candidate for the next generational solar cell due to their outstanding optoelectronic properties and rapid development in recent years. However, the biggest challenge to prevent them from massive commercial use is their long-term stability. Photoemission spectroscopy has been widely used to investigate properties of the perovskites, which provide critical insights to better understand the degradation mechanisms. In this article, we review mainly our photoemission studies on the degradation processes of perovskite thin films and single crystals with different environmental factors, such as gases, water, and light by monitoring changes of chemical composition and electronic structure. These studies on the effects by different environmental parameters are discussed for the understanding of the stability issues and the possible solutions.

Keywords: photoemission spectroscopy (PES); perovskite thin films; perovskite single crystals; environmental stability

Citation: Wang, K.; Ecker, B.; Gao, Y. Photoemission Studies on the Environmental Stability of Thermal Evaporated $MAPbI_3$ Thin Films and $MAPbBr_3$ Single Crystals. *Energies* **2021**, *14*, 2005. https://doi.org/10.3390/en14072005

Academic Editors: Massimo Viviani and Emmanuel Kymakis

Received: 26 January 2021
Accepted: 17 March 2021
Published: 5 April 2021

1. Introduction

Since the first application in photovoltaic cells in 2009 [1]. Organic−inorganic halide perovskites have received considerable attention and have been the focus of the enormous research effort in the past few years due to their outstanding performance in optoelectronic devices. The power conversion efficiency (PCE) of the perovskite solar cells (PSCs) raised from 3.8% in 2009 [1] to 25.5% in 2020 [2] only for a decade of development, given their superb properties such as long diffusion length, long carrier lifetime, tunable bandgap and high absorption coefficient [3–7]. In addition, ease of fabrication and low production cost make them competitive to the traditional silicon-based solar cells [8,9]. With these unique features, PSCs are a suitable choice for the next generation of photovoltaic devices. Although the performance of the PSCs has been heavily investigated, the long-term stability is still the biggest concern in the research community that prevents them from further commercial applications.

There are a lot of factors that limit the stability and performance of perovskites, like moisture, oxygen, light irradiation, which have been found and investigated by the research community. Niu et al. found that $CH_3NH_3PbI_3$ ($MAPbI_3$) could degrade in the presence of moisture and Al_2O_3 could successfully protect the perovskite layer [10]. Aristidou et al. reported that $MAPbI_3$ photoactive layers rapidly decompose into CH_3NH_2, PbI_2, and I_2 after oxygen and light exposure, which is triggered by the reaction of superoxide (O_2^-) with the $CH_3NH_3^+$ cation from the perovskite absorber [11]. Philippe et al. studied performance of both $MAPbI_{3-x}Cl_x$ and $MAPbI_3$ under higher temperatures. The perovskite films were heated in an ultra-high vacuum (UHV) chamber without the presence of air and moisture and degraded when the temperature approached 100 °C [12]. Lee et al. observed UV degradation on PSCs after a 1000-h exposure of 365 nm UV light under inert gas at

<0.5 ppm humidity without encapsulation [13]. Nie et al. showed their PSCs formed light-activated meta-stable trap states under constant light illumination, which is caused by photocurrent degradation [14]. In addition to the MA-based perovskite, Formamidinium (FA) based perovskites have been reported more stable than pure MA-based perovskites under high temperature, as the molar mass of FA is larger than MA [15,16]

There are also investigations on other factors, such as Iodine vapor, voltage, device structure and mechanical stress [17–21]. On device level, Eperon et al. found that $FAPbI_3$ substrate showed higher stability as compared to $MAPbI_3$ when both were heated at 150 °C [15]. Lee. et al. showed that oxygen does not harm the stability of the PSCs as they were stored in the dark [22]. The most commonly used hole transporting material, spiroOMeTAD is unstable in the presence of water which could cause the decomposition of the PSCs [23]. Leijtens et al. observed that PSCs tend to degrade under light illumination which could decrease short-circuit current density (J_{sc}) [21]

To improve the stability and the performance of the PSCs, it is essential to have a better cognition not only on the device level but also on the material level. However, most previous stability works were based on the observation of device performance, which is usually focused on the parameters including open-circuit voltage (V_{oc}), J_{sc}, fill factor (FF), and PCE [24–28]. These parameters are often monitored in a function of time to measure the stability of the device. The reduction of these parameters usually results from the degradation of the perovskites, but the degradation mechanism did not receive attention as much as the device performance. Therefore, the study of the surface level of the electronic and chemical properties of the perovskites is necessary to help develop possible solutions for the stability issues.

There is a number of choices of method to grow perovskites: spin coating, spray coating, chemical vapor deposition (CVD), physical vapor deposition (PVD), thermal evaporation, blade coating, and screen printing [29–35]. Spin coating is a simple method to fabricate thin films and is widely used to quickly and easily synthesize perovskites in a lab environment [27,36–40]. The PSC with high efficiency of 24.8% was achieved with spin coating method [41]. Besides, it has been applied to fabricate large-scale perovskite photovoltaic devices [42]. However, a more suitable way for environmental tests is thermal evaporation. Studies showed that evaporated perovskite films have a more uniform surface, fewer defects, and more ideal chemical stoichiometry [43–48]. Besides, the thin films are prepared in the vacuum system which can be processed for the measurements right after the film growth without being exposed to the ambient environment. Similar to evaporated thin films, the in situ cleaved perovskite single crystals (SCs) are also suitable for the degradation measurements [49]. Crystallinity plays an important role in the degradation process. Since the disorder of material was increased by the defects on surfaces, voids, and grain boundaries thus weaken the bonding, degradation would be more severe where the defects exist. In this case, studies show that moisture and thermal stability of the perovskite material can be increased by the surface and grain boundary passivation [50,51]. Therefore, better crystallinity is preferred for the studies on degradation.

Photoemission spectroscopy (PES) is one of the most suitable and widely used techniques to probe the chemical and electronic properties of a material [52]. As explained by Einstein in 1905, photoelectrons are generated by the interaction between the irradiating photons and the sample [53]. The schematic of PES is shown in Figure 1a. The incident photons excite electrons which can be detected by an electron energy analyzer, if the excited electrons have enough energy to leave the sample and escape to the vacuum. The kinetic energy of the excited electrons is E_K, and it is expressed by the following equation [54]:

$$E_K = h\nu - E_B - \Phi \quad (1)$$

where $h\nu$ is the photon energy, E_B is the binding energy (BE) of the electron with respect to the Fermi level, and the work function is represented by Φ which is the minimum energy needed to move an electron from solid to the vacuum.

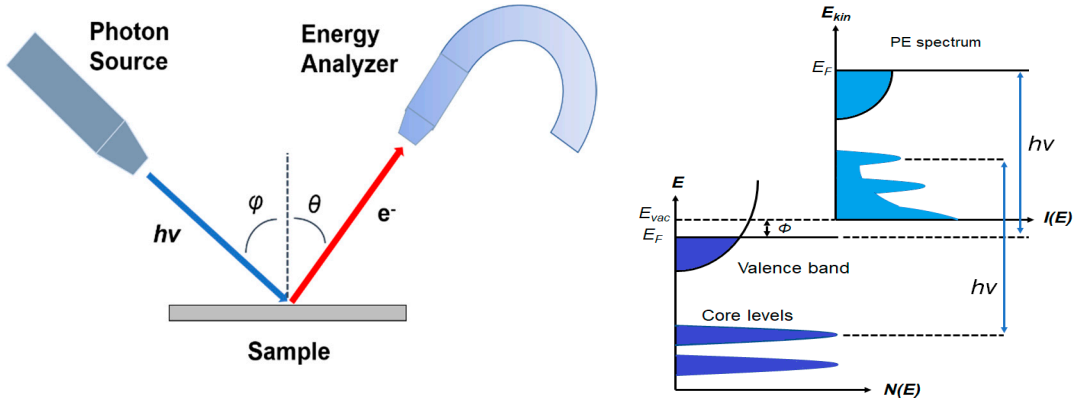

Figure 1. (**a**) Schematic of a photoemission experiment. (**b**) Schematic representation of photoemission spectroscopy (PES). From Ref. [47] with permission.

The schematic of PES is shown in Figure 1b, which demonstrates that PES detects photoelectrons from occupied states, including the valence bands (VB) and the core-level states, depends on the photon energy it uses. Also, the vacuum level cutoff is defined by the secondary electrons excited by the photoelectrons [55].

PES is highly surface sensitive as a surface analytic tool, which uses photoexcited electrons as the probing particles. These electrons have a strong interaction with the solid, resulting in a shorter escape distance, known as the mean free path (MFP). The MFP is the average distance that the particles can travel before colliding with another particle, which is highly determined by the kinetic energy of the photoelectron and has less material dependency [56]. The thickness of a monolayer is typically ranging from 0.2–0.4 nm in different materials.

X-ray photoemission spectroscopy (XPS) is a most commonly used PES technique to investigate the performance of semiconductor materials [57]. MFP of XPS is less than 10.0 nm and as an in-situ technique with high surface sensitivity, it has been widely used to monitor compositional change on the surface which is caused by degradation [58–60]. Detailed control of the exposure measurements is able to be performed within the UHV system.

In this review, we present a comprehensive overview of our quantitative studies on environmental factors, such as oxygen, moisture, X-ray, and illumination, that affect the stability of both thermal evaporated $MAPbI_3$ thin film and $MAPbBr_3$ single crystal. We further obtain insights into the intrinsic degradation mechanisms based on the compositional and structural changes during the measurements. Suggestions are also proposed to improve the long-term stability of PSCs in the future.

2. Environmental Stability of Perovskite Thin Films

2.1. Air Exposure on $MAPbI_3$ Thin Film

The 60 nm thick evaporated $MAPbI_3$ thin film was exposed to the ambient air for ~24 h at room temperature (RT) and relative humidity (RH) of 25%. The total thickness of the perovskite layer was determined by the reading of quartz crystal microbalance during the sample growth process. Figure 2 shows the XPS spectrum that before and after the exposure [46]. Only C, N, I and Pb peaks can be observed and no other elemental features can be found in Figure 2a. The elemental ratio of C:N:Pb:I:O is 1.29:1.07:1.00:2.94:0 which was similar to the ideal stoichiometry of $MAPbI_3$ and better to those from spin-coated ones. These again proved the high quality of the thermal evaporated thin film. For the perovskite thin film after air exposure, the red marks show the appearance of gold and oxygen peaks, and the blue mark stands for the disappearance of the N 1s peak. Therefore, the ratio changed to C:N:Pb:I:O = 2.22:0:1.00:1.26:0.58. This can be attributed to the absorption of moisture from the environment, thus caused the film to degrade into PbI_2. It has also been

reported that $MAPbI_3$ film became less n-type after a 15-min exposure to ambient air [61]. The XPS used in this study has an MFP of ~2 nm, which unable to detect the underlying gold substrate. In this case, gold signal may suggest that the sample was heavily roughened by air exposure to the gold layer.

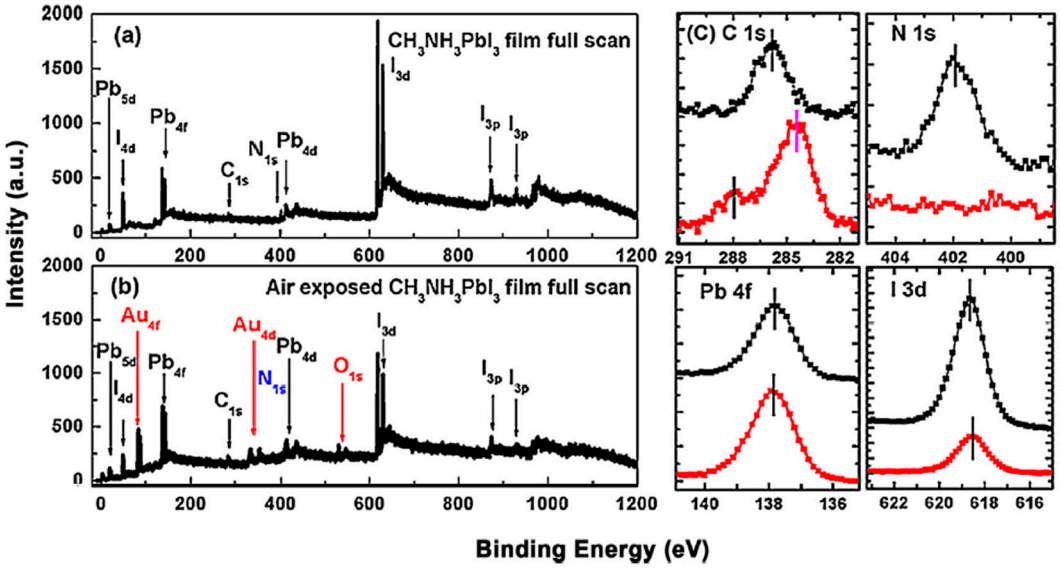

Figure 2. (**a**) XPS full scan of co-evaporated $MAPbI_3$ thin film and (**b**) XPS full scan of air-exposed film. (**c**) XPS spectra comparisons of C 1s, N 1s, Pb 4f, and I 3d core levels. From Ref. [35] with permission.

However, the effects of air exposure are controversial since some reports show that moderate exposure to ambient air could improve crystallinity, grain size, carrier mobility, and charge carrier lifetime of perovskites, thus leading to a better performance of PSCs [62–64]. This is contrasted with our observation and the claim that moisture in the air can accelerate the degradation of perovskites [65,66].

2.2. Oxygen Exposure on $MAPbI_3$ Thin Film

Oxygen, as the second-largest composition of air, is considered a potential trigger of perovskite degradation. There are several studies showed that moisture and oxygen could affect the performance of PSCs severely. Sun et al. observed that oxygen-induced degradation is triggered at the surfaces and grain boundaries, which is irreversible and can occur at oxygen levels as low as 1% under light illumination [67]. However, most reports focused on the effects of oxygen and moisture together, while this work discusses the effects from each factor independently.

XPS core level spectra of the $MAPbI_3$ film under O_2 exposure and dry air exposure are shown in Figure 3 [47]. Langmuir (L, 1 L = 10^{-6} Torr·s) is used to measure gas adsorption in a UHV system as a unit of exposure to a surface. No obvious change was observed during the exposure in terms of peak positions and intensities. No oxygen signal can be found even after 10^{13} L of exposure. There is also no apparent change in the BEs of C 1s, I 3d, and Pb 4f [47]. The valence band maximum (VBM) slightly moved from 0.85 to 0.67 eV after 10^{13} L of exposure, suggesting that oxygen may serve as a p-type dopant without changing the structure of the film. This can be explained that oxygen photogenerated electrons from the perovskite as an acceptor, leading to the formation of superoxide (O_2^-) species or the reduction of the metallic Pb-related surface states [11,61,68]. From these spectra, it can be seen that there is no change of the film composition and structure without the presence of moisture. These results indicate that the evaporated film is inert to oxygen. Similarly, Ralairosa et al. also observed shifts of the VBM to lower BE during oxygen exposure, which agrees with our observation [61]. Kim et al. also confirmed that minimal oxygen exposure does not damage the final perovskite structure [69].

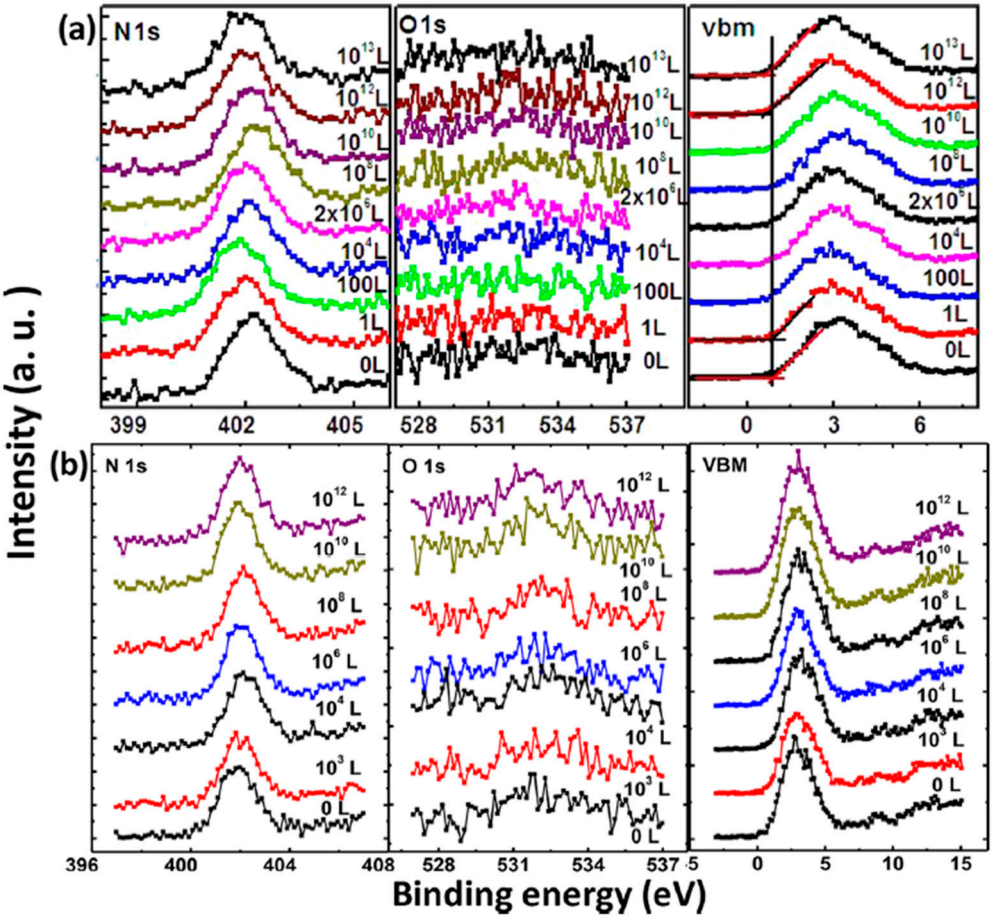

Figure 3. XPS spectra of N 1s, O 1s, and the VBM region of co-evaporated $MAPbI_3$ thin film during (**a**) oxygen exposure and (**b**) dry air exposure From Ref. [37] with permission.

2.3. Water Exposure on $MAPbI_3$ Thin Film

Based on the observations above, we learned that water is the most concerned environmental factor that initiates the degradation process of perovskites. To have more insight of the mechanism behind water-induced degradation, air exposure and water exposure monitored with XPS in a well-controlled sequence are shown in Figure 4. Air exposure was conducted at RT and RH of 41%. The spectra were normalized to the same height in order to be compared properly except for those of N 1s because the signal vanished as the exposure proceed. Both structural and compositional trends of the two measurements are similar. There is no significant change of the spectral shape for perovskite carbon peak C 1s-A and nitrogen peak N 1s before 60 min of air exposure and 1×10^{10} L of water exposure (Stage one); there is only a rigid shift toward the higher BE region. O 1s peak intensity was not increasing in this stage either. In Figure 4b, after 1×10^{10} L of water exposure, Fermi level moved from 0.85 to 1.41 eV in the VBM region and almost reached the bottom of the conduction band (CB) as the bandgap of $MAPbI_3$ is 1.55 eV [47]. This indicates that water heavily n-doped perovskite in this stage, while the integrity of the sample remains unchanged. This has been related to the metallic Pb surface defects and the position of E_F in the bandgap sensitively shifts with the density of these surface states [70,71]. Besides, a density of state develop at 6.5 eV indicates the formation of the metallic Pb, leading to an irreversible degradation [72,73].

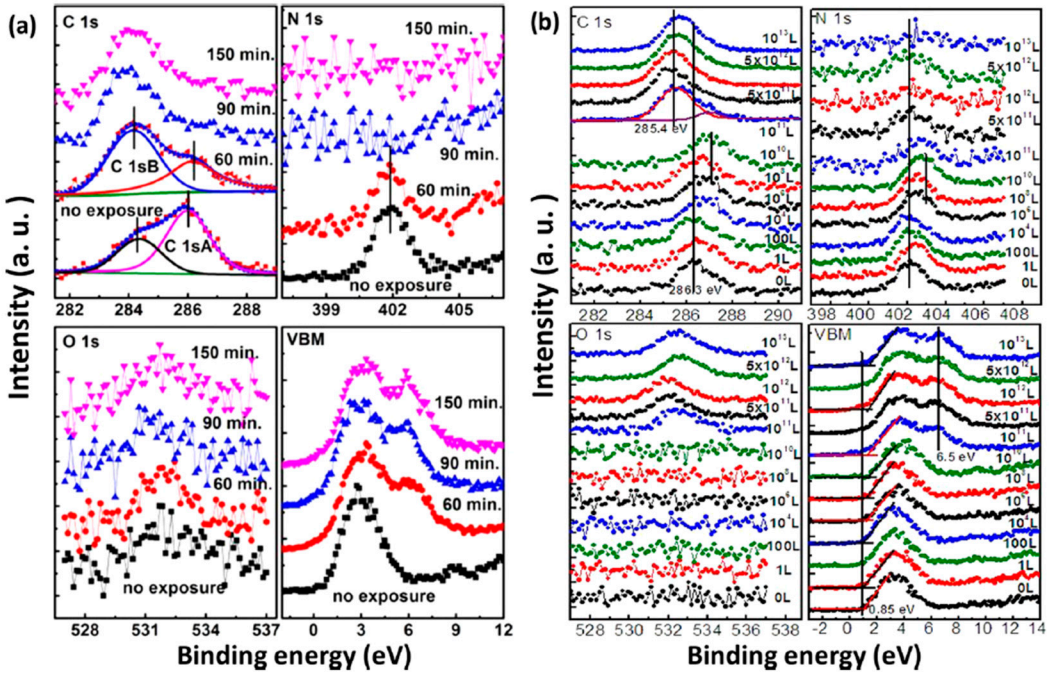

Figure 4. XPS spectral evolutions of C 1s, N 1s, O 1s, and the VBM region of evaporated $MAPbI_3$ thin film during (**a**) atmospheric air exposure and (**b**) H_2O exposure. From Ref. [37] with permission.

The sample was observed to have dramatic change after 60 min of air exposure and 1×10^{10} L of water exposure (stage two). In the air exposure, the intensity of perovskite carbon peak C 1s-A started to decrease, while amorphous carbon peak C 1s-B and leftover carbon from the degradation of perovskite began to increase. In water exposure, C 1s peak shifted from 286.3 eV (MA^+) to 285.4 eV, which represents the decomposition of MA^+ into hydrocarbon complex. After 90 min and 5×10^{11} L of exposure of air and water, the carbon from perovskite was almost disappeared. Similarly, N 1s signal was gone after 150 min and 10^{12} L of exposure to air and water, respectively, while the O 1s peak from water adsorption appeared and developed significantly. The movement of the O 1s position in Figure 3b is a firm indication of chemical reactions. A broad peak at around 6.5 eV in the VBM region showed up and became sharper over time, suggesting the presence of water on the sample surface in stage two. There is almost no change in the intensity of Pb 4f, while the I/Pb ratio dropped to 2.1 when the exposure ended. These show that water in the air triggers the decomposition of perovskite.

Based on the discussion above, the degradation mechanism of the evaporated $MAPbI_3$ thin film under air exposure was expressed as

$$CH_3NH_3PbI_3 \overset{H_2O}{\rightarrow} (-CH_2-) + PbI_2 + NH_3\uparrow + HI\uparrow \quad (2)$$

The reaction between $MAPbI_3$ and H_2O results in a hydrocarbon complex (most likely polyethylene-like (−CH2−CH2−)) [74]. PbI_2, and absorbed water. Nitrogen and part of Iodine left the surface as gases. This agrees well with water catalytic model proposed by other groups [10,75]. The degradation process is irreversible as the gaseous species leave the sample surface. However, it has been reported that perovskite monohydrate phase was identified with in-situ grazing-incidence X-ray diffraction (GIXRD) after ~170 min exposure to RH over 80%, which could be attributed to water physisorption [73].

By combining the time of air exposure and the water exposure level, the threshold of water degradation can be obtained. The RH of the atmospheric air was 41% and the saturated vapor pressure is ~18.650 Torr at RT [76]. Thus, the 60 min exposure amount of ambient air can be calculated as $0.41 \times 60 \times 60$ s $\times$ 18.650 Torr = 2.75×10^{10} L, which

is consistent with the threshold between 10^{10} and 10^{11} L in water exposure. It can be concluded that water only acts as an n-dopant before $\sim 2 \times 10^{10}$ L of water exposure, while starts to react with the sample and destroy the structure of perovskite beyond the exposure level. In addition to the PES study, XRD measurements also showed a similar degradation process which further confirmed the mechanism [47].

2.4. Light Exposure on $MAPbI_3$ Thin Film

Besides the environmental factors discussed above, light illumination is also another potential trigger of decomposing the perovskite and a number of researchers have been studying this issue. Leijtens et al. claimed that the light-induced degradation of PSCs can be attributed to the TiO_2 layer in the device [17]. Murugadoss et al. revealed a strong substrate dependence of perovskite thin films [77]. Bryant et al. studied perovskite stability in gases and ambient environment and found that light illumination was the main factor causing the degradation [78]. Das et al. also reported that the chemical properties of their spin-coated $MAPbI_3$ film change upon illumination in vacuum with the formation of metallic Pb and then by conversion into PbI_2. These changes can be restricted by applying an extraction voltage to the device contacts which leads to the extraction of the photogenerated charges from the absorber [79]. Zhao et al. found that $MAPbI_3$ thin films are strained which is caused by the mismatched thermal expansion during the annealing process, thus increases ion migration in strained perovskites films and accelerates degradation of perovskite films under light illumination [80]. Yuan et al. showed that ion migration caused by electric current can accelerate the decomposition of $MAPbI_3$ [81]

The photostability investigation of the $MAPbI_3$ thin film with XPS is shown in Figure 5. The laser has a wavelength of 408 nm and the intensity is ~7 times the AM 1.5 irradiation [82]. For the laser irradiated spot, all peaks began to shift to the higher BE region after 120 min of light exposure and saturated after 480 min. There is a 0.4 eV increase in the VBM after 2210 min of illumination, which agrees with the idea that the film became more n-type during the exposure. A new Pb component showed up at 136.87 eV after 120 min of illumination, which is synchronized with the new feature in the VBM region at 6.5 eV. This new Pb peak represents a new chemical component and was caused metallic Pb to form, which has previously been reported at 137.0 eV for the Pb $4f_{7/2}$ and was synchronized with the new peak at 6.5 eV in the VBM region [83,84]. About 33% of the total Pb converted to metallic Pb after the exposure. The intensity of the N 1s and I 3d were also reduced during irradiation. With these observations, it is clear that the film was first decomposed into PbI_2 by light irradiation and was further degraded into metallic Pb and iodine. Therefore, excess Pb may cause the sample became n-doping, which is similar to the high temperature annealing of perovskite [43]. The metallic Pb can heavily limit the performance of the device by acting as a quenching center of excitons. For the nonirradiated spot, there is no obvious change for all the peaks.

The light-induced degradation process discussed above can be expressed as the two following steps [82]

$$CH_3NH_3PbI_3 \overset{\text{Light}}{\rightarrow} (-CH_2-) + PbI_2 + NH_3 \uparrow + HI \uparrow \quad (3)$$

$$PbI_2 \overset{\text{Light}}{\rightarrow} Pb + I_2 \uparrow \quad (4)$$

The volatile species, NH_3 and HI leave the surface in the first step, and so does the iodine in the second step by sublimation, leaving the remaining $MAPbI_3$, metallic Pb, and hydrocarbon complex components on the surface. This is also observed by other groups [11,85]. In contrast, Das et al. suggested that photodegradation of $MAPbI_3$ film occurs in two steps in vacuum. First, iodine vacancies were created by vacuum in perovskite, then light-induced charge carriers react with perovskite, forming organic dissociates. These iodine vacancies can trap the photogenerated electrons before the recombination, then Pb^{2+} could acquire the electron and convert to metallic Pb [79,86]. The vacuum could also accelerate the removal of the volatile species from the perovskite. However, in various

literature, it has been reported that the metallic Pb can convert back to perovskite when rest in the dark and cation migration in the dark can enhance the decreased performance of the PSCs [14,87].

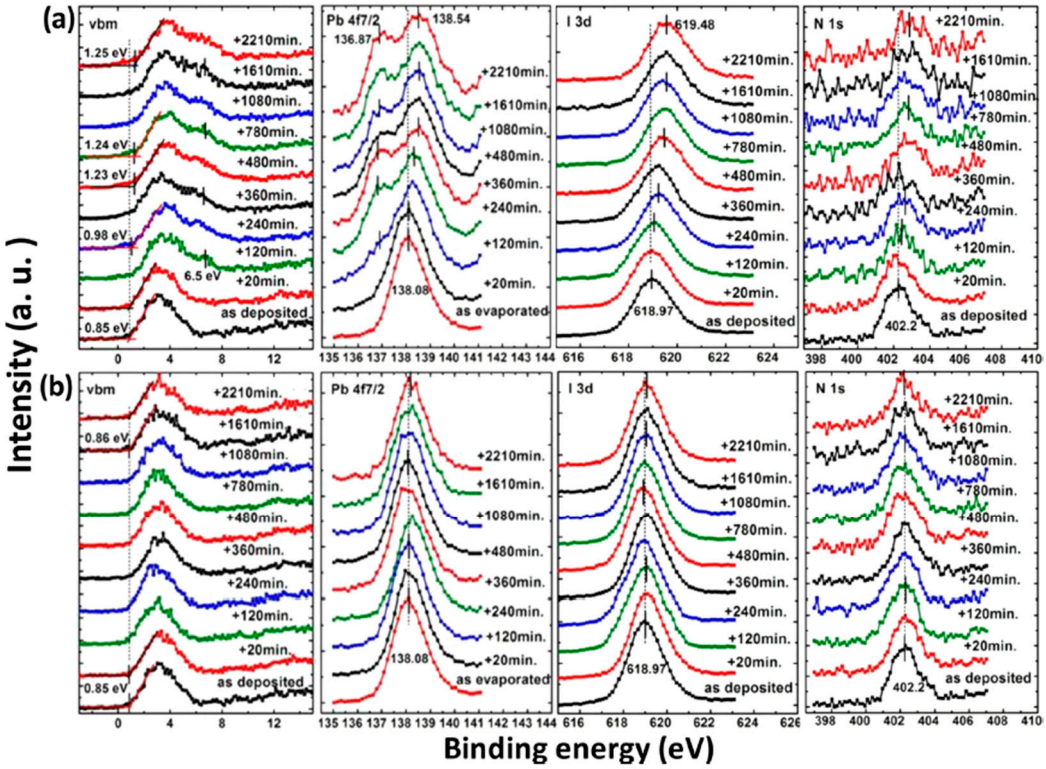

Figure 5. XPS spectra of co-evaporated $MAPbI_3$ thin film at (**a**) laser irradiated and (**b**) nonirradiated positions. From Ref. [54] with permission.

3. Environmental Stability of Perovskite Single Crystals

3.1. X-ray Exposure on $MAPbBr_3$ Single Crystal

In Figure 6a, a second Pb component (Pb-B) started to show up at ~136.04 eV from the second scan as marked by the red arrow, which is identified as the metallic Pb, while the perovskite Pb-A peak is at ~138.05 eV. As shown in Figure 7, the core level of all elements has no significant change, except for Pb.

A possible reaction is proposed to explain the conversion of metallic Pb under X-ray exposure [49].

$$CH_3NH_3PbBr_3 \overset{X-ray}{\rightarrow} CH_3NH_3Br + Pb + Br_2 \uparrow \quad (5)$$

By comparing the elemental ratios of the whole process, 10% Pb-A converted to Pb-B, which suggests that 10% of the perovskite decomposed after 10-h X-ray exposure. C 1s peak position is ~285.81 eV and no amorphous carbon showed up at ~284.6 eV at either the test spot (Figure 7) or the control spot (Figure S1 (see supplementary materials)). It shows that the increased carbon was not from the contamination in the UHV chamber, which may suggest that it could be attributed to the surface diffusion of MABr.

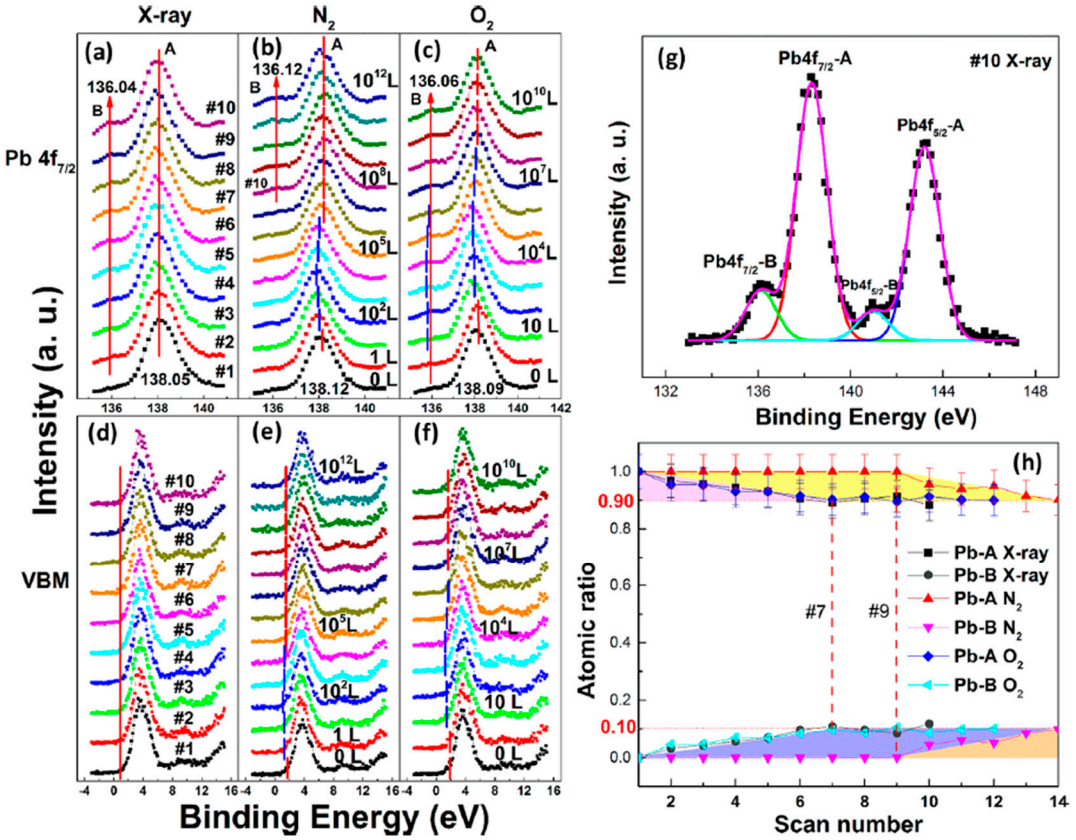

Figure 6. (**a**–**f**) XPS spectral evolutions of Pb 4f7/2 and VBM of cleaved MAPbBr3 single crystal under X-ray, N2, and O2 exposures, respectively. (**g**) The detailed fitting curves for Pb under the 10th X-ray scan. (**h**) Elemental ratio comparisons of Pb peaks under the three conditions with error bars. From Ref. [38] with permission.

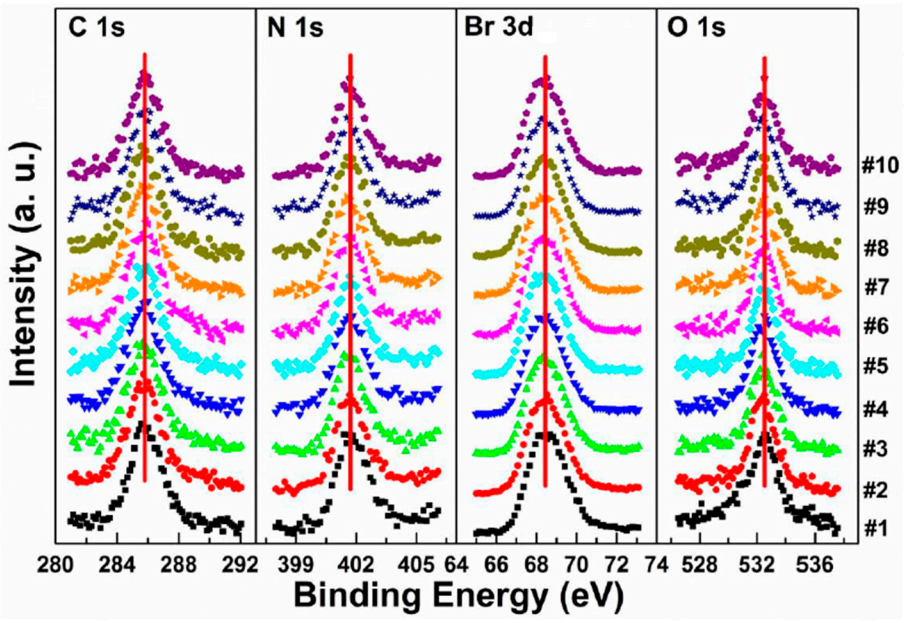

Figure 7. Evolutions of C 1s, N 1s, Br 3d, and O 1s XPS spectra of cleaved $MAPbBr_3$ single crystal under X-ray exposure. From Ref. [38] with permission.

3.2. Nitrogen Exposure on $MAPbBr_3$ Single Crystal

Although N_2 is normally used to protect the sample as an inert gas during the perovskite environmental studies [66,88–90]. the role of N_2 in the degradation process remains to be clarified.

Figure 6b,e and Figure 8 are associated with N_2 exposure. Before 10^7 L, it can be observed that all peaks and VBM started to move toward the low BE direction and reach the maximum at 10^2 L by about 0.31 eV, then shifted back to the original position at 10^5 L. This represents that the perovskite crystal was slightly p-doped by nitrogen via physical absorption and N_2 slowly left the surface afterward. There is no metallic Pb nor other elemental ratio change at 10^7 L with 9-h X-ray exposure, suggesting that the sample surface can be protected from X-ray degradation with N_2 for up to 9 h and stop MABr diffusion at the same time. However, metallic Pb peak started to show up at 10^8 L and increased to 10% of the total Pb at 10^{12} L (14-h XPS scan). The degradation process is the same as discussed in Equation (5). It can be concluded that N_2 could protect perovskite crystal from XPS X-ray degradation for 9 h as it p-doped perovskite by ~0.31 eV first then slowly left the surface.

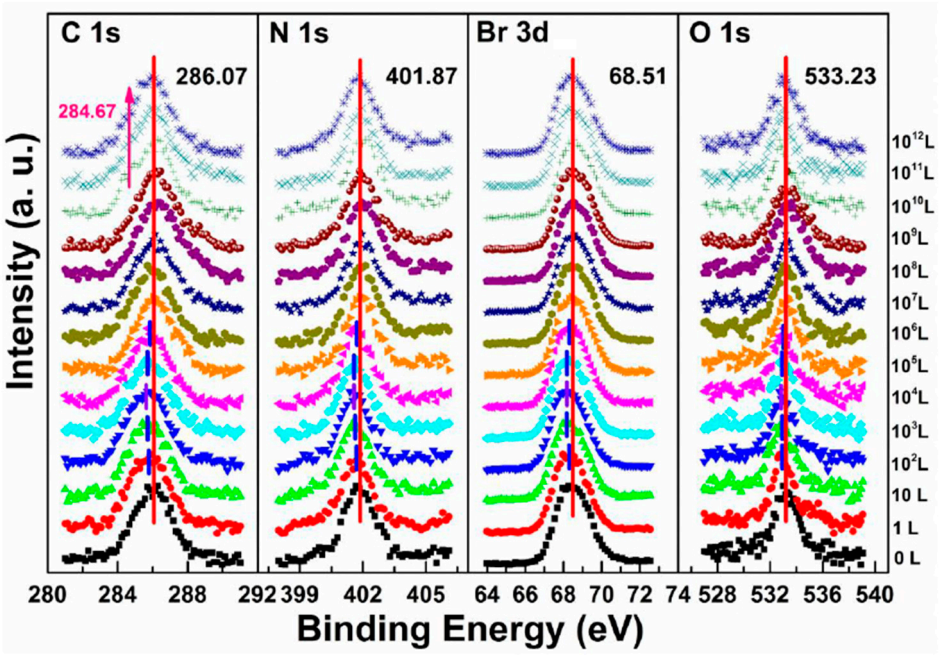

Figure 8. Evolutions of C 1s, N 1s, Br 3d, and O 1s XPS spectra of cleaved $MAPbBr_3$ single crystal under N_2 exposures. From Ref. [38] with permission.

3.3. Oxygen Exposure on $MAPbBr_3$ Single Crystal

In the previous discussion of perovskite thin films, O_2 does not react with the sample and only acts as a p-dopant during the exposure. It's also important to know if it acts the same with perovskite SCs.

The metallic Pb peak began to develop from the second scan as under the X-ray exposure, which suggests that O_2 cannot shield the sample as N_2 did under the same condition, as shown in Figure 6c,f. The peak position and the ratio changes indicate that the exposure process consists two steps. In step one, all peaks started to move to the lower BE direction from 1 L and reached the maximum at 10^4 L, except O 1s. The VBM also had the same pattern with a maximum shift of ~0.18 eV, which is the same as the oxygen exposure on perovskite thin films [47]. Meanwhile, O 1s started to move to the higher BE region from the beginning and achieved the maximum of ~534.09 eV at 10^4 L. These firmly suggested that the detected O 1s mostly came from the crystal surface by O_2 p-doping.

Figure 9 shows that a second carbon peak at ~287.71 eV (C 1s-B) and a second oxygen peak at ~532.56 eV (O 1s-B) appeared after 10^4 L in step two, which indicates the doped oxygen started to bond with carbon and formed C−O bond, at 10^{10} L. Other peaks began to move back to their original positions as the doped O_2 decreased. It is noted that carbon which bonded with oxygen came from MABr due to X-ray degradation and also from MA^+ diffusion. Similar to perovskite thin film, perovskite SC also does not react with O_2.

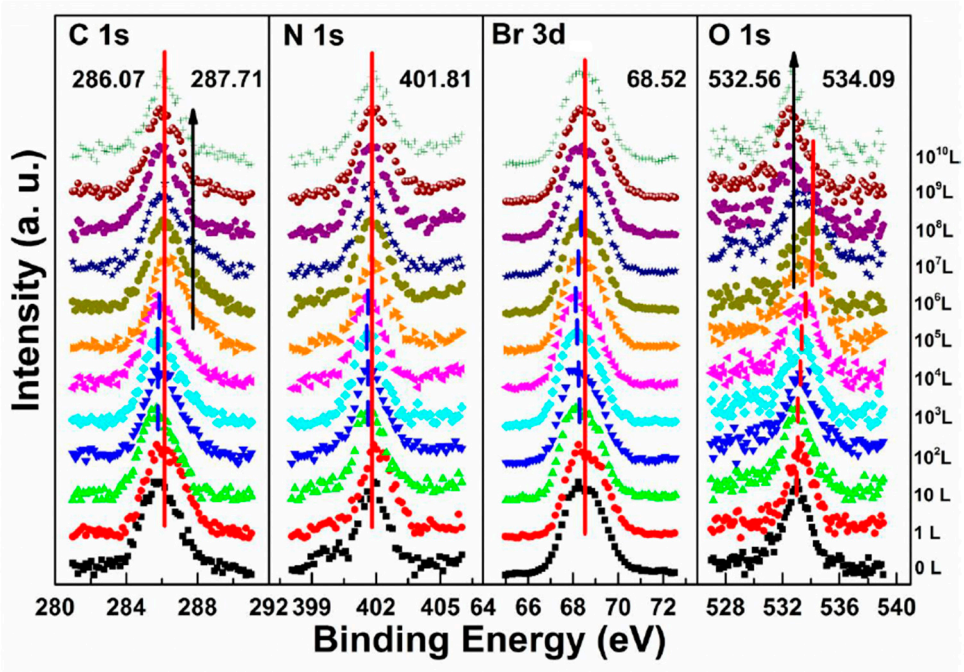

Figure 9. Evolutions of C 1s, N 1s, Br 3d, and O 1s XPS spectra of cleaved $MAPbBr_3$ single crystal under O_2 exposures. From Ref. [38] with permission.

By comparing the metallic Pb ratios from the three atmospheres, it can be found that no matter when the degradations started and how long the exposures were, the ratio of the metallic Pb always saturated at 10%. This may be because that the perovskite surface was covered by the 10% metallic Pb layer which prevented it from further decomposition. It has been reported that $MAPbBr_3$ single crystal has better stability and can be stored in air for eight months [91–93]. In addition, oxygen exposure could enhance photoluminescence (PL) performance of the $MAPbBr_3$ single crystal [94].

3.4. Water Exposure on $MAPbBr_3$ Single Crystal

Similar to the perovskite thin film, perovskite SC may also vulnerable to moisture. Figure 10 shows the evolution of five major elements and the VB region. The whole exposure process can also be divided into two stages.

In stage one, there was a rigid shift of ~0.24 eV to the higher BE direction for carbon, nitrogen, bromine, and lead peaks before 10^8 L. The rigid shift indicates that water worked as an n-dopant, causing the Fermi level of the crystal to move from 1.53 eV to 1.77 eV. The metallic Pb peak appeared at ~136.08 eV from the second scan which was caused by X-ray degradation. There is no obvious signal for oxygen from the freshly cleaved sample and the oxygen peak started to show up at ~533.00 eV from 10^3 L, which can be attributed to water. Then it moved toward the lower BE direction with a maximum of ~0.18 eV at 10^8 L. This displacement in opposite direction indicates that there was no chemical reaction between water and the SC during this stage.

The ratio is C/N/Pb/Br/O = 1.53:1.10:1:2.92: for the freshly cleaved $MAPbBr_3$ SC. The same 10% ratio of Pb from perovskite converted into metallic Pb at the end of the first stage (10^8 L of H_2O), as the net change under 7 h exposure of X-ray. However, the ratios

of C 1s, N 1s, and Br $3d_{5/2}$ dropped by ~30, 37, and 27%, respectively, and doped water caused a 14% increase in O 1s. In addition to Equation (5), the following mechanism is proposed for step one in water exposure [49].

$$CH_3NH_3Br \xrightarrow{H_2O+\ X-ray} CH_3NH_2(g)\ +\ HBr\uparrow \quad (6)$$

There is ~30% MABr from the diffusion and the X-ray degradation further decomposed into CH_3NH_2 and HBr gases under X-ray with 14% doped water and then escaped the sample surface.

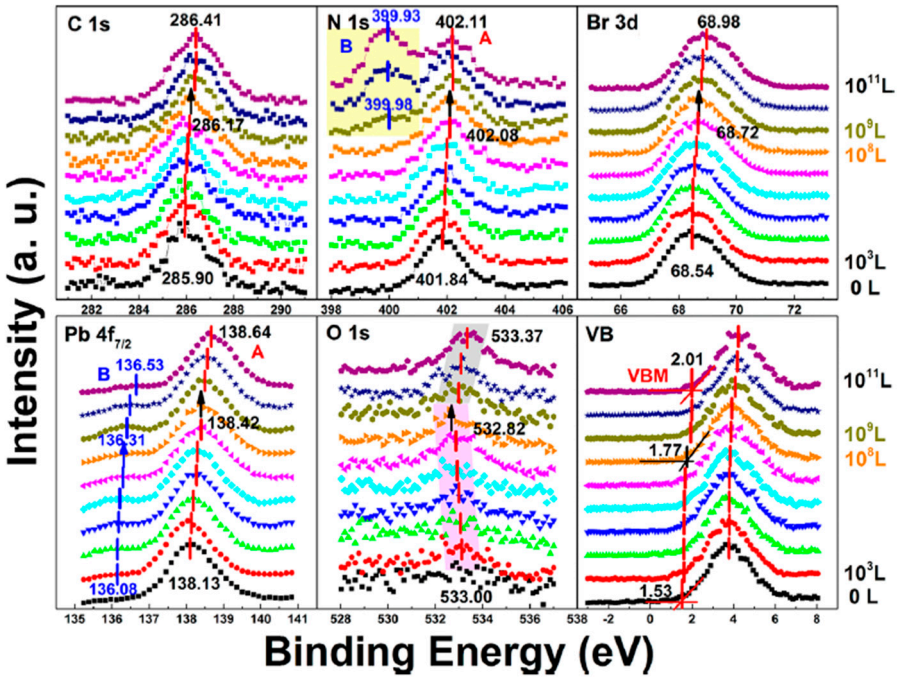

Figure 10. Evolution of C 1s, N 1s, Br 3d, Pb $4f_{7/2}$, O 1s, and the VB region of cleaved $MAPbBr_3$ single crystal under water exposure from 0 to 10^{11} L. From Ref. [38] with permission.

In the second stage, $MAPbBr_3$ SC started to react with water from 10^9 L as two noticeable changes are shown in Figure 10. First, the O 1s quickly moved to the higher BE direction by ~0.55 eV, which was the same for the other major peaks but opposite from that before 10^8 L. The oxygen peak at ~533.37 eV (10^{11} L) may come from hydroxide. C 1s, Br $3d_{5/2}$, two Pb peaks, and VBM all shifted ~0.24 eV to the higher BE during the period. Second, there was a second nitrogen peak (N 1s-B) showed up at ~399.98 eV, which may be caused by NH_4^+ formed by the reaction of NH_3 and H_2O. It slightly shifted ~0.05 eV to the lower BE direction, while perovskite nitrogen peak N 1s-A kept moving to the higher BE until achieving ~402.11 eV at 10^{11} L. These results strongly demonstrate that water was a key factor causing decomposition of perovskite SC in the second step. After the exposure, Fermi level was moved to 0.29 eV, as the bandgap is 2.3 eV for the $MAPbBr_3$ SC, which indicates a very n-type doping.

Metallic Pb increased 17% while the saturate ratio is only 10% under the same X-ray exposure condition. The extra metallic Pb may attribute to X-ray degradation of $PbBr_2$, which is from $MAPbBr_3$ and water reaction. After 10^{10} L, carbon increased ~40%, while nitrogen and bromine decreased ~39 and 32%, respectively, exposure level. Therefore, the following reactions were proposed in stage two [49].

$$CH_3NH_3PbBr_3 \xrightarrow{H_2O} (-CH_2-)\ +\ PbBr_2\ +\ NH_3\uparrow\ +\ HBr\uparrow \quad (7)$$

$$PbBr_2 \overset{X-ray}{\rightarrow} Pb + Br_2 \uparrow \quad (8)$$

$$2Pb + 2H_2O + O_2 \rightarrow 2Pb(OH)_2 \downarrow \quad (9)$$

This degradation mechanism is very similar to Equation (2). of the $MAPbI_3$ thin films. About 35% perovskite was decomposed into HBr and NH_3 gases by water in UHV. Partial ammonia was absorbed by water, while $PbBr_2$ was further decomposed into metallic Pb and Br_2. From 10^{10} L, white precipitate $Pb(OH)_2$ was formed by the reaction of metallic Pb, water and the residual oxygen in the chamber. Bulk crystal could be intact with some water molecules and reversible photoelectrical properties [94]. However, PL confirmed the doping of the H_2O molecules, thus leading to the lattice distortion-induced reconstruction of the SC [95].

3.5. Light Exposure on $MAPbBr_3$ Single Crystal

The stability of $MAPbBr_3$ SC under light illumination was investigated with a blue laser, which has a wavelength of 408 nm and intensity is ~7 times the AM 1.5 irradiation. The exposed spot received a total light exposure time of 44 h. Strong chemical decomposition was observed with XPS after the light exposure. It has been reported that structural changes in the perovskite lattice were observed under illumination, which is related to the light-induced ion migration and associated defect passivation [96]. Anaya et al. reported that by combining in situ PL and XPS analysis, they found the formation of a negatively charged layer of adsorbed anionic oxygen species on the surface which could drive halide anions away from the illuminated areas toward the bulk of the material [97].

A new metallic Pb spectral component started to show up in the Pb core level spectra as shown in Figure 11. The original perovskite Pb $4f_{7/2}$ and $4f_{5/2}$ peaks were located at 138.27 and 143.17 eV, respectively. A new metallic Pb feature started to appear for each Pb core level after light exposure. Both the metallic and the perovskite Pb peaks moved to a lower BE which occurred within the first hour of light exposure. C, N, and Br peaks also had a similar initial BE movement as shown in Figure 12. This rigid shift is corresponding to the Fermi level movement within the bandgap, which suggests the perovskite was p doped.

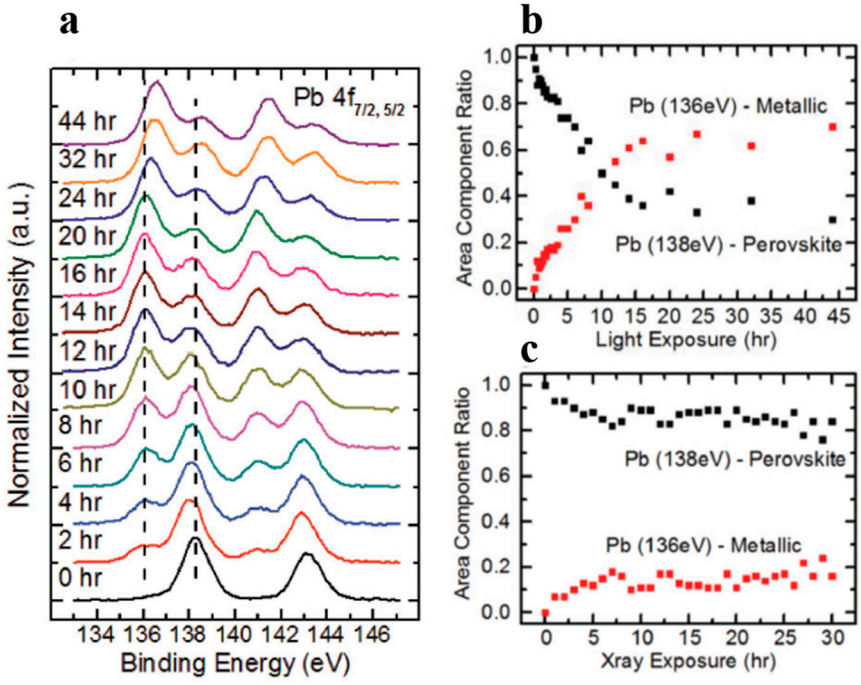

Figure 11. (**a**) A stack plot of the Pb $4f_{7/2}$ and $4f_{5/2}$ core levels of cleaved $MAPbBr_3$ single crystal with increasing light exposure. (**b**,**c**) The ratio of perovskite Pb to metallic Pb under light exposure and X-ray exposure, respectively. From Ref. [62] with permission.

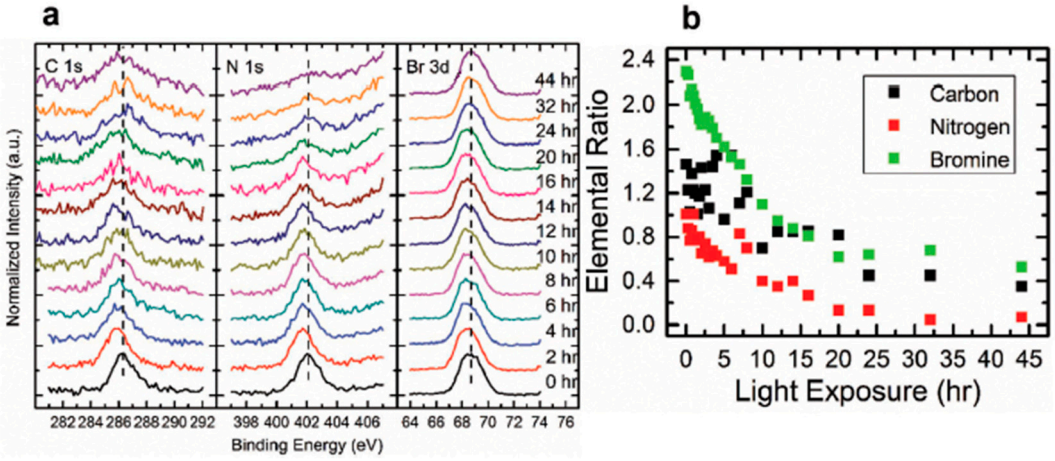

Figure 12. (**a**) A stack plot of the C 1s, N 1s, Br $3d_{5/2}$ core levels of cleaved $MAPbBr_3$ single crystal with increasing light exposure. (**b**) Elemental ratio change for C, N, and Br under light exposure. From Ref. [62] with permission.

After the initial BE shift, all peaks started to gradually shift back to higher BEs and the metallic Pb peaks stopped at ~136.6 and 141.4 eV for the $4f_{7/2}$ and $4f_{5/2}$ core levels, respectively. As the light exposure progressed, the metallic Pb component continued to gain in intensity and finally dominated the overall Pb core level after ~10 h of exposure. When the whole 44 h exposure was finished, ~70% of Pb signal came from the metallic Pb, while only ~30% signal was the perovskite Pb.

For all other elements, there were no new features observed during the exposure, which suggests that they did not change their chemical states. However, the surface saw noticeable concentration losses in C, N, and Br. In Figure 12, at ~10 h of light exposure, C, N, and Br lost about half of their initial concentration, and ~50% of the perovskite Pb was degraded into metallic Pb. Based on these observations, the following mechanism was proposed to explain the degradation process [98].

$$CH_3NH_3PbBr_3 \overset{\text{Light}}{\rightarrow} CH_3NH_3Br + PbBr_2 \quad (10)$$

$$PbBr2 \overset{\text{Light}}{\rightarrow} Pb + Br_2 \quad (11)$$

The perovskite SC first degraded into MABr and $PbBr_2$, then $PbBr_2$ further degrade into metallic Pb and Br_2 under light exposure. C, N, and Br were decomposed as volatile species, then escape the sample surface similar to simple outgassing. Interestingly, a similar degradation process was also observed under E-Beam Irradiation [99].

4. Summary

Long-term stability is one of the most critical challenges for emerging perovskite materials. Despite enormous efforts were put into the research of improving the stability of PSCs, there is still a long way to go to achieve their commercialization. In this article, the environmental factors that limit the stability of both perovskite thin film and perovskite SC under ambient environments have been reviewed. With PES techniques, these environmental studies have been performed and analyzed quantitatively and systematically, then the detailed electronic structure and composition changes of the perovskite surface were revealed. The surface analysis shows that perovskite thin film is not sensitive to N_2 and O_2, while water and light could quickly destroy the perovskite structure once the exposure passes a certain threshold. For perovskite SC, X-ray degradation is mild and inevitable when the sample was measured with XPS. N_2 was able to protect the SC from X-ray damage for 9 h and O_2 could bond with C to form C−O. Similar to the thin film, SC is also vulnerable to water and light, which could trigger severe damage to the structure and change the chemical composition.

It is critical to understand and improve the intrinsic stability of perovskites under different environmental conditions. Therefore, these works provide detailed observation and analysis of the degradation mechanisms which would help to obtain high-efficiency PSCs with better environmental stability.

Supplementary Materials: This figure is available online at: https://www.mdpi.com/article/10.3390/en14072005/s1.

Funding: The work received financial support from National Science Foundation, grant number DMR-1903962.

Data Availability Statement: No new data is reported in this review.

Acknowledgments: B.E. acknowledges Hooker Dissertation Fellowship from the University of Rochester. The authors would like to acknowledge Jinsong Huang for providing CH_3NH_3I powder and $MAPbI_3$ single crystals. They would also like to acknowledge Youzhen Li and Congcong Wang for their earlier work.

Conflicts of Interest: The authors declare no conflict of interest.

References

1. Kojima, A.; Teshima, K.; Shirai, Y.; Miyasaka, T. Organometal halide perovskites as visible-light sensitizers for photovoltaic cells. *J. Am. Chem. Soc.* **2009**, *131*, 6050–6051. [CrossRef]
2. National Renewable Energy Laboratory. Best Research-Cell Efficiency Chart. Available online: https://www.nrel.gov/pv/cell-efficiency.html (accessed on 28 September 2020).
3. Xie, H.; Liu, X.; Lyu, L.; Niu, D.; Wang, Q.; Huang, J.; Gao, Y. Effects of Precursor Ratios and Annealing on Electronic Structure and Surface Composition of CH3NH3PbI3 Perovskite Films. *J. Phys. Chem. C* **2015**, *120*, 215–220. [CrossRef]
4. Kim, H.S.; Lee, C.R.; Im, J.H.; Lee, K.B.; Moehl, T.; Marchioro, A.; Moon, S.J.; Humphry-Baker, R.; Yum, J.H.; Moser, J.E.; et al. Lead iodide perovskite sensitized all-solid-state submicron thin film mesoscopic solar cell with efficiency exceeding 9%. *Sci. Rep.* **2012**, *2*, 591. [CrossRef]
5. Dunlap-Shohl, W.A.; Younts, R.; Gautam, B.; Gundogdu, K.; Mitzi, D.B. Effects of Cd Diffusion and Doping in High-Performance Perovskite Solar Cells Using CdS as Electron Transport Layer. *J. Phys. Chem. C* **2016**, *120*, 16437–16445. [CrossRef]
6. Abrusci, A.; Stranks, S.D.; Docampo, P.; Yip, H.L.; Jen, A.K.; Snaith, H.J. High-performance perovskite-polymer hybrid solar cells via electronic coupling with fullerene monolayers. *Nano Lett.* **2013**, *13*, 3124–3128. [CrossRef]
7. Stranks, S.D.; Eperon, G.E.; Grancini, G.; Menelaou, C.; Alcocer, M.J.; Leijtens, T.; Herz, L.M.; Petrozza, A.; Snaith, H.J. Electron-hole diffusion lengths exceeding 1 micrometer in an organometal trihalide perovskite absorber. *Science* **2013**, *342*, 341–344. [CrossRef]
8. Guerrero, A.; Juarez-Perez, E.J.; Bisquert, J.; Mora-Sero, I.; Garcia-Belmonte, G. Electrical field profile and doping in planar lead halide perovskite solar cells. *Appl. Phys. Lett.* **2014**, *105*, 133902. [CrossRef]
9. Lunardi, M.M.; Ho-Baillie, A.; Alvarez-Gaitan, J.P.; Moore, S.; Corkish, R. A life cycle assessment of perovskite/silicon tandem solar cells. *Prog. Photovoltaics Res. Appl.* **2017**, *25*, 679–695. [CrossRef]
10. Niu, G.; Li, W.; Meng, F.; Wang, L.; Dong, H.; Qiu, Y. Study on the stability of CH 3 NH 3 PbI 3 films and the effect of post-modification by aluminum oxide in all-solid-state hybrid solar cells. *J. Mater. Chem. A* **2014**, *2*, 705–710. [CrossRef]
11. Aristidou, N.; Sanchez-Molina, I.; Chotchuangchutchaval, T.; Brown, M.; Martinez, L.; Rath, T.; Haque, S.A. The role of oxygen in the degradation of methylammonium lead trihalide perovskite photoactive layers. *Angew. Chem.* **2015**, *127*, 8326–8330. [CrossRef]
12. Philippe, B.; Park, B.-W.; Lindblad, R.; Oscarsson, J.; Ahmadi, S.; Johansson, E.M.; Rensmo, H.K. Chemical and Electronic Structure Characterization of Lead Halide Perovskites and Stability Behavior under Different Exposures—A Photoelectron Spectroscopy Investigation. *Chem. Mater.* **2015**, *27*, 1720–1731. [CrossRef]
13. Lee, S.-W.; Kim, S.; Bae, S.; Cho, K.; Chung, T.; Mundt, L.E.; Lee, S.; Park, S.; Park, H.; Schubert, M.C. UV degradation and recovery of perovskite solar cells. *Sci. Rep.* **2016**, *6*, 1–10. [CrossRef] [PubMed]
14. Nie, W.; Blancon, J.-C.; Neukirch, A.J.; Appavoo, K.; Tsai, H.; Chhowalla, M.; Alam, M.A.; Sfeir, M.Y.; Katan, C.; Even, J.; et al. Light-activated photocurrent degradation and self-healing in perovskite solar cells. *Nat. Commun.* **2016**, *7*, 1–9. [CrossRef]
15. Eperon, G.E.; Stranks, S.D.; Menelaou, C.; Johnston, M.B.; Herz, L.M.; Snaith, H.J.; Science, E. Formamidinium lead trihalide: A broadly tunable perovskite for efficient planar heterojunction solar cells. *Energy Environ. Sci.* **2014**, *7*, 982–988. [CrossRef]
16. Lee, J.W.; Kim, D.H.; Kim, H.S.; Seo, S.W.; Cho, S.M.; Park, N.-G. Formamidinium and cesium hybridization for photo-and moisture-stable perovskite solar cell. *Adv. Energy Mater.* **2015**, *5*, 1501310. [CrossRef]
17. Wang, S.; Jiang, Y.; Juarez-Perez, E.J.; Ono, L.K.; Qi, Y.B. Accelerated degradation of methylammonium lead iodide perovskites induced by exposure to iodine vapour. *Nat. Energy* **2017**, *2*, 16195. [CrossRef]
18. Xiao, Z.; Yuan, Y.; Shao, Y.; Wang, Q.; Dong, Q.; Bi, C.; Sharma, P.; Gruverman, A.; Huang, J. Giant switchable photovoltaic effect in organometal trihalide perovskite devices. *Nat. Mater.* **2015**, *14*, 193–198. [CrossRef]

19. Boyd, C.C.; Cheacharoen, R.; Leijtens, T.; McGehee, M.D. Understanding degradation mechanisms and improving stability of perovskite photovoltaics. *Chem. Rev.* **2018**, *119*, 3418–3451. [CrossRef]
20. Rolston, N.; Printz, A.D.; Tracy, J.M.; Weerasinghe, H.C.; Vak, D.; Haur, L.J.; Priyadarshi, A.; Mathews, N.; Slotcavage, D.J.; McGehee, M.D. Effect of cation composition on the mechanical stability of perovskite solar cells. *Adv. Energy Mater.* **2018**, *8*, 1702116. [CrossRef]
21. Leijtens, T.; Eperon, G.E.; Pathak, S.; Abate, A.; Lee, M.M.; Snaith, H.J. Overcoming ultraviolet light instability of sensitized TiO2 with meso-superstructured organometal tri-halide perovskite solar cells. *Nat. Commun.* **2013**, *4*, 1–8. [CrossRef]
22. Lee, M.M.; Teuscher, J.; Miyasaka, T.; Murakami, T.N.; Snaith, H.J. Efficient hybrid solar cells based on meso-superstructured organometal halide perovskites. *Science* **2012**, *338*, 643–647. [CrossRef]
23. Suarez, B.; Gonzalez-Pedro, V.; Ripolles, T.S.; Sanchez, R.S.; Otero, L.; Mora-Sero, I. Recombination study of combined halides (Cl, Br, I) perovskite solar cells. *J. Phys. Chem. Lett.* **2014**, *5*, 1628–1635. [CrossRef]
24. Son, D.-Y.; Lee, J.-W.; Choi, Y.J.; Jang, I.-H.; Lee, S.; Yoo, P.J.; Shin, H.; Ahn, N.; Choi, M.; Kim, D.; et al. Self-formed grain boundary healing layer for highly efficient CH 3 NH 3 PbI 3 perovskite solar cells. *Nat. Energy* **2016**, *1*, 1–8. [CrossRef]
25. Jeon, N.J.; Noh, J.H.; Yang, W.S.; Kim, Y.C.; Ryu, S.; Seo, J.; Seok, S.-I. Compositional engineering of perovskite materials for high-performance solar cells. *Nat. Cell Biol.* **2015**, *517*, 476–480. [CrossRef] [PubMed]
26. Yang, W.S.; Noh, J.H.; Jeon, N.J.; Kim, Y.C.; Ryu, S.; Seo, J.; Seok, S.-I. High-performance photovoltaic perovskite layers fabricated through intramolecular exchange. *Science* **2015**, *348*, 1234–1237. [CrossRef]
27. Edri, E.; Kirmayer, S.; Cahen, D.; Hodes, G. High open-circuit voltage solar cells based on organic-inorganic lead bromide perovskite. *J. Phys. Chem. Lett.* **2013**, *4*, 897–902. [CrossRef]
28. Baikie, T.; Fang, Y.; Kadro, J.M.; Schreyer, M.; Wei, F.; Mhaisalkar, S.G.; Graetzel, M.; White, T.J. Synthesis and crystal chemistry of the hybrid perovskite (CH 3 NH 3) PbI 3 for solid-state sensitised solar cell applications. *J. Mater. Chem. A* **2013**, *1*, 5628–5641. [CrossRef]
29. Im, J.-H.; Lee, C.-R.; Lee, J.-W.; Park, S.-W.; Park, N.-G. 6.5% efficient perovskite quantum-dot-sensitized solar cell. *Nanoscale* **2011**, *3*, 4088–4093. [CrossRef]
30. Barrows, A.T.; Pearson, A.J.; Kwak, C.K.; Dunbar, A.D.; Buckley, A.R.; Lidzey, D.G.; Science, E. Efficient planar heterojunction mixed-halide perovskite solar cells deposited via spray-deposition. *Energy Environ. Sci.* **2014**, *7*, 2944–2950. [CrossRef]
31. Tavakoli, M.M.; Gu, L.; Gao, Y.; Reckmeier, C.; He, J.; Rogach, A.L.; Yao, Y.; Fan, Z. Fabrication of efficient planar perovskite solar cells using a one-step chemical vapor deposition method. *Sci. Rep.* **2015**, *5*, 14083. [CrossRef]
32. Lan, C.; Dong, R.; Zhou, Z.; Shu, L.; Li, D.; Yip, S.; Ho, J.C. Large-scale synthesis of freestanding layer-structured PbI2 and MAPbI3 nanosheets for high-performance photodetection. *Adv. Mater.* **2017**, *29*, 1702759. [CrossRef]
33. Qin, P.; Tanaka, S.; Ito, S.; Tetreault, N.; Manabe, K.; Nishino, H.; Nazeeruddin, M.K.; Grätzel, M. Inorganic hole conductor-based lead halide perovskite solar cells with 12.4% conversion efficienc. *Nat. Commun.* **2014**, *5*, 1–6. [CrossRef]
34. Deng, Y.; Peng, E.; Shao, Y.; Xiao, Z.; Dong, Q.; Huang, J.J.E.; Science, E. Scalable fabrication of efficient organolead trihalide perovskite solar cells with doctor-bladed active layers. *Energy Environ. Sci.* **2015**, *8*, 1544–1550. [CrossRef]
35. Cao, K.; Zuo, Z.; Cui, J.; Shen, Y.; Moehl, T.; Zakeeruddin, S.M.; Grätzel, M.; Wang, M. Efficient screen printed perovskite solar cells based on mesoscopic TiO2/Al2O3/NiO/carbon architecture. *Nano Energy* **2015**, *17*, 171–179. [CrossRef]
36. Zheng, L.; Ma, Y.; Chu, S.; Wang, S.; Qu, B.; Xiao, L.; Chen, Z.; Gong, Q.; Wu, Z.; Hou, X. Improved light absorption and charge transport for perovskite solar cells with rough interfaces by sequential deposition. *Nanoscale* **2014**, *6*, 8171–8176. [CrossRef]
37. Ma, Y.; Zheng, L.; Chung, Y.-H.; Chu, S.; Xiao, L.; Chen, Z.; Wang, S.; Qu, B.; Gong, Q.; Wu, Z.; et al. A highly efficient mesoscopic solar cell based on CH 3 NH 3 PbI 3− x Cl x fabricated via sequential solution deposition. *Chem. Commun.* **2014**, *50*, 12458–12461. [CrossRef] [PubMed]
38. Kazim, S.; Nazeeruddin, M.K.; Grätzel, M.; Ahmad, S. Perovskite as light harvester: A game changer in photovoltaics. *Angew. Chem. Int. Ed.* **2014**, *53*, 2812–2824. [CrossRef] [PubMed]
39. Chen, W.; Wu, Y.; Yue, Y.; Liu, J.; Zhang, W.; Yang, X.; Chen, H.; Bi, E.; Ashraful, I.; Grätzel, M. Efficient and stable large-area perovskite solar cells with inorganic charge extraction layers. *Science* **2015**, *350*, 944–948. [CrossRef] [PubMed]
40. Ito, S.; Tanaka, S.; Vahlman, H.; Nishino, H.; Manabe, K.; Lund, P. Carbon-double-bond-free printed solar cells from TiO2/CH3NH3PbI3/CuSCN/Au: Structural control and photoaging effects. *ChemPhysChem* **2014**, *15*, 1194–1200. [CrossRef]
41. Jeong, M.; Choi, I.W.; Go, E.M.; Cho, Y.; Kim, M.; Lee, B.; Jeong, S.; Jo, Y.; Choi, H.W.; Lee, J.; et al. Stable perovskite solar cells with efficiency exceeding 24.8% and 0.3-V voltage loss. *Science* **2020**, *369*, 1615–1620.
42. Han, G.S.; Kim, J.; Bae, S.; Han, S.; Kim, Y.J.; Gong, O.Y.; Lee, P.; Ko, M.K.; Jung, H.S. Spin-coating process for 10 cm× 10 cm perovskite solar modules enabled by self-assembly of SnO2 nanocolloids. *ACS Energy Lett.* **2019**, *4*, 1845–1851. [CrossRef]
43. Wang, Q.; Shao, Y.; Xie, H.; Lyu, L.; Liu, X.; Gao, Y.; Huang, J. Qualifying composition dependent p and n self-doping in CH3NH3PbI3. *Appl. Phys. Lett.* **2014**, *105*, 163508. [CrossRef]
44. Liu, M.; Johnston, M.B.; Snaith, H.J. Efficient planar heterojunction perovskite solar cells by vapour deposition. *Nature* **2013**, *501*, 395–398. [CrossRef] [PubMed]
45. Xiao, Z.; Bi, C.; Shao, Y.; Dong, Q.; Wang, Q.; Yuan, Y.; Wang, C.; Gao, Y.; Huang, J. Efficient, high yield perovskite photovoltaic devices grown by interdiffusion of solution-processed precursor stacking layers. *Energy Environ. Sci.* **2014**, *7*, 2619–2623. [CrossRef]

46. Wang, C.; Li, Y.; Xu, X.; Wang, C.; Xie, F.; Gao, Y. Degradation of co-evaporated perovskite thin film in air. *Chem. Phys. Lett.* **2016**, *649*, 151–155. [CrossRef]
47. Li, Y.; Xu, X.; Wang, C.; Wang, C.; Xie, F.; Yang, J.; Gao, Y. Degradation by Exposure of Coevaporated CH3NH3PbI3 Thin Films. *J. Phys. Chem. C* **2015**, *119*, 23996–24002. [CrossRef]
48. Wang, C.; Gao, Y. Stability of perovskites at the surface analytic level. *J. Phys. Chem. Lett.* **2018**, *9*, 4657–4666. [CrossRef] [PubMed]
49. Wang, C.; Ecker, B.R.; Wei, H.; Huang, J.; Gao, Y. Environmental Surface Stability of the MAPbBr3 Single Crystal. *J. Phys. Chem. C* **2018**, *122*, 3513–3522. [CrossRef]
50. Abdelmageed, G.; Sully, H.R.; Bonabi Naghadeh, S.; El-Hag Ali, A.; Carter, S.A.; Zhang, J.Z. Improved stability of organometal halide perovskite films and solar cells toward humidity via surface passivation with oleic acid. *ACS Appl. Energy Mater.* **2018**, *1*, 387–392. [CrossRef]
51. Park, C.; Ko, H.; Sin, D.H.; Song, K.C.; Cho, K. Organometal halide perovskite solar cells with improved thermal stability via grain boundary passivation using a molecular additive. *Adv. Funct. Mater.* **2017**, *27*, 1703546. [CrossRef]
52. Hüfner, S. *Photoelectron Spectroscopy: Principles and Applications*; Springer Science & Business Media: Berlin/Heidelberg, Germany, 2013.
53. Einstein, A. Concerning an heuristic point of view toward the emission and transformation of light. *Am. J. Phys.* **1965**, *33*, 367.
54. Park, R.L.; Lagally, M.G. *Solid State Physics: Surfaces*; Academic Press: Cambridge, MA, USA, 1985; Volume 22.
55. Reinert, F.; Hüfner, S. Photoemission spectroscopy—From early days to recent applications. *New J. Phys.* **2005**, *7*, 97. [CrossRef]
56. Seah, M.P.; Dench, W.A. Quantitative electron spectroscopy of surfaces: A standard data base for electron inelastic mean free paths in solids. *Surf. Interface Anal.* **1979**, *1*, 2. [CrossRef]
57. Li, Y.; Xu, X.; Wang, C.; Wang, C.; Xie, F.; Yang, J.; Gao, Y. Investigation on thermal evaporated CH3NH3PbI3 thin films. *AIP Adv.* **2015**, *5*, 097111. [CrossRef]
58. Wang, K.; Ecker, B.; Gao, Y. Angle-Resolved Photoemission Study on the Band Structure of Organic Single Crystals. *Crystals* **2020**, *10*, 773. [CrossRef]
59. Wang, C.; Irfan, I.; Liu, X.; Gao, Y. Role of molybdenum oxide for organic electronics: Surface analytical studies. *J. Vac. Sci. Technol. B Nanotechnol. Microelectron. Mater. Process. Meas. Phenom.* **2014**, *32*, 040801. [CrossRef]
60. Wang, C.; Liu, X.; Wang, C.; Kauppi, J.; Gao, Y. Electronic structure evolution in doping of fullerene (C60) by ultra-thin layer molybdenum trioxide. *J. Appl. Phys.* **2015**, *118*, 085304. [CrossRef]
61. Ralaiarisoa, M.; Salzmann, I.; Zu, F.-S.; Koch, N. Effect of water, oxygen, and air exposure on CH3NH3PbI3–xClx perovskite surface electronic properties. *Adv. Electron. Mater.* **2018**, *4*, 1800307. [CrossRef]
62. Eperon, G.E.; Habisreutinger, S.N.; Leijtens, T.; Bruijnaers, B.J.; van Franeker, J.J.; DeQuilettes, D.W.; Pathak, S.; Sutton, R.J.; Grancini, G.; Ginger, D.S.; et al. The importance of moisture in hybrid lead halide perovskite thin film fabrication. *ACS Nano* **2015**, *9*, 9380–9393. [CrossRef]
63. You, J.; Yang, Y.; Hong, Z.; Song, T.-B.; Meng, L.; Liu, Y.; Jiang, C.; Zhou, H.; Chang, W.-H.; Li, G.; et al. Moisture assisted perovskite film growth for high performance solar cells. *Appl. Phys. Lett.* **2014**, *105*, 183902. [CrossRef]
64. Dubey, A.; Kantack, N.; Adhikari, N.; Reza, K.M.; Venkatesan, S.; Kumar, M.; Khatiwada, D.; Darling, S.; Qiao, Q. Room temperature, air crystallized perovskite film for high performance solar cells. *J. Mater. Chem. A* **2016**, *4*, 10231–10240. [CrossRef]
65. Shirayama, M.; Kato, M.; Miyadera, T.; Sugita, T.; Fujiseki, T.; Hara, S.; Kadowaki, H.; Murata, D.; Chikamatsu, M.; Fujiwara, H. Degradation mechanism of CH3NH3PbI3 perovskite materials upon exposure to humid air. *J. Appl. Phys.* **2016**, *119*, 115501. [CrossRef]
66. Yang, J.; Siempelkamp, B.D.; Liu, D.; Kelly, T.D. Investigation of CH3NH3PbI3 degradation rates and mechanisms in controlled humidity environments using in situ techniques. *ACS Nano* **2015**, *9*, 1955–1963. [CrossRef]
67. Sun, Q.; Fassl, P.; Becker-Koch, D.; Bausch, A.; Rivkin, B.; Bai, S.; Hopkinson, P.E.; Snaith, H.J.; Vaynzof, Y. Role of microstructure in oxygen induced photodegradation of methylammonium lead triiodide perovskite films. *Adv. Energy Mater.* **2017**, *7*, 1700977. [CrossRef]
68. Aristidou, N.; Eames, C.; Sanchez-Molina, I.; Bu, X.; Kosco, J.; Islam, M.S.; Haque, S.A. Fast oxygen diffusion and iodide defects mediate oxygen-induced degradation of perovskite solar cells. *Nat. Commun.* **2017**, *8*, 15218. [CrossRef]
69. Kim, J.; Schelhas, L.T.; Stone, K.H. Effects of Oxygen and Water on the Formation and Degradation Processes of (CH3NH3) PbI3 Thin Films. *ACS Appl. Energy Mater.* **2020**, *3*, 11269–11274. [CrossRef]
70. Conings, B.; Baeten, L.; De Dobbelaere, C.; D'Haen, J.; Manca, J.; Boyen, H.G. Perovskite-based hybrid solar cells exceeding 10% efficiency with high reproducibility using a thin film sandwich approach. *Adv. Mater.* **2014**, *26*, 2041–2046. [CrossRef]
71. Zu, F.S.; Amsalem, P.; Salzmann, I.; Wang, R.B.; Ralaiarisoa, M.; Kowarik, S.; Duhm, S.; Koch, N. Impact of white light illumination on the electronic and chemical structures of mixed halide and single crystal perovskites. *Adv. Opt. Mater.* **2017**, *5*, 1700139. [CrossRef]
72. Christians, J.A.; Miranda Herrera, P.A.; Kamat, P.V. Transformation of the excited state and photovoltaic efficiency of CH3NH3PbI3 perovskite upon controlled exposure to humidified air. *J. Am. Chem. Soc.* **2015**, *137*, 1530–1538. [CrossRef] [PubMed]
73. Leguy, A.M.; Hu, Y.; Campoy-Quiles, M.; Alonso, M.I.; Weber, O.J.; Azarhoosh, P.; Van Schilfgaarde, M.; Weller, M.T.; Bein, T.; Nelson, J.; et al. Reversible hydration of CH3NH3PbI3 in films, single crystals, and solar cells. *Chem. Mater.* **2015**, *27*, 3397–3407. [CrossRef]

74. Nist X-Ray Photoelectron Spectroscopy Database. Available online: http://Srdata.Nist.Gov/Xps/Default.Aspx (accessed on 17 December 2020).
75. Ke, J.C.-R.; Walton, A.S.; Lewis, D.J.; Tedstone, A.; O'Brien, P.; Thomas, A.G.; Flavell, W.R. In situ investigation of degradation at organometal halide perovskite surfaces by X-ray photoelectron spectroscopy at realistic water vapour pressure. *Chem. Commun.* **2017**, *53*, 5231–5234.
76. Weast, R.C.; Astle, M.J.; Beyer, W.H. (Eds.) *CRC Handbook of Chemistry and Physics*; CRC Press: Boca Raton, FL, USA, 1985.
77. Murugadoss, G.; Tanaka, S.; Mizuta, G.; Kanaya, S.; Nishino, H.; Umeyama, T.; Imahori, H.; Ito, S. Light stability tests of methylammonium and formamidinium Pb-halide perovskites for solar cell applications. *Jpn. J. Appl. Phys.* **2015**, *54*, 08KF08. [CrossRef]
78. Bryant, D.; Aristidou, N.; Pont, S.; Sanchez-Molina, I.; Chotchunangatchaval, T.; Wheeler, S.; Durrant, J.R.; Haque, S.A. Light and oxygen induced degradation limits the operational stability of methylammonium lead triiodide perovskite solar cells. *Energy Environ. Sci.* **2016**, *9*, 1655–1660. [CrossRef]
79. Das, C.; Wussler, M.; Hellmann, T.; Mayer, T.; Jaegermann, W. In situ XPS study of the surface chemistry of MAPI solar cells under operating conditions in vacuum. *Phys. Chem. Chem. Phys.* **2018**, *20*, 17180–17187. [CrossRef]
80. Zhao, J.; Deng, Y.; Wei, H.; Zheng, X.; Yu, Z.; Shao, Y.; Shield, J.E.; Huang, J. Strained hybrid perovskite thin films and their impact on the intrinsic stability of perovskite solar cells. *Sci. Adv.* **2017**, *3*, eaao5616. [CrossRef]
81. Yuan, H.; Debroye, E.; Janssen, K.; Naiki, H.; Steuwe, C.; Lu, G.; Moris, M.I.; Orgiu, E.; Uji-i, H.; De Schryver, F.; et al. Degradation of methylammonium lead iodide perovskite structures through light and electron beam driven ion migration. *J. Phys. Chem. Lett.* **2016**, *7*, 561–566. [CrossRef]
82. Li, Y.Z.; Xu, X.R.; Wang, C.C.; Ecker, B.; Yang, J.L.; Huang, J.; Gao, Y.L. Light-Induced Degradation of CH3NH3PbI3 Hybrid Perovskite Thin Film. *J. Phys. Chem. C* **2017**, *121*, 3904–3910. [CrossRef]
83. Sadoughi, G.; Starr, D.E.; Handick, E.; Stranks, S.D.; Gorgoi, M.; Wilks, R.G.; Bär, M.; Snaith, H.J. Observation and mediation of the presence of metallic lead in organic-inorganic perovskite films. *ACS Appl. Mater. Interfaces* **2015**, *7*, 13440–13444. [CrossRef]
84. Liu, L.; McLeod, J.A.; Wang, R.; Shen, P.; Duhm, S. Tracking the formation of methylammonium lead triiodide perovskite. *Appl. Phys. Lett.* **2015**, *107*, 061904. [CrossRef]
85. Huang, W.; Manser, J.S.; Kamat, P.V.; Ptasinska, S. Evolution of chemical composition, morphology, and photovoltaic efficiency of CH3NH3PbI3 perovskite under ambient conditions. *Chem. Mater.* **2016**, *28*, 303–311. [CrossRef]
86. Tang, X.; Brandl, M.; May, B.; Levchuk, I.; Hou, Y.; Richter, M.; Chen, H.; Chen, S.; Kahmann, S.; Osvet, A.; et al. Photoinduced degradation of methylammonium lead triiodide perovskite semiconductors. *J. Mater. Chem. A* **2016**, *4*, 15896–15903. [CrossRef]
87. Domanski, K.; Roose, B.; Matsui, T.; Saliba, M.; Turren-Cruz, S.-H.; Correa-Baena, J.-P.; Carmona, C.R.; Richardson, G.; Foster, J.M.; De Angelis, F.; et al. Migration of cations induces reversible performance losses over day/night cycling in perovskite solar cells. *Energy Environ. Sci.* **2017**, *10*, 604–613. [CrossRef]
88. Dong, X.; Fang, X.; Lv, M.; Lin, B.; Zhang, S.; Ding, J.; Yuan, N. Improvement of the humidity stability of organic-inorganic perovskite solar cells using ultrathin Al2O3 layers prepared by atomic layer deposition. *J. Mater. Chem. A* **2015**, *3*, 5360–5367. [CrossRef]
89. Wang, Y.-K.; Yuan, Z.-C.; Shi, G.-Z.; Li, Y.-X.; Li, Q.; Hui, F.; Sun, B.-Q.; Jiang, Z.-Q.; Liao, L.-S. Dopant-free spiro-triphenylamine/fluorene as hole-transporting material for perovskite solar cells with enhanced efficiency and stability. *Adv. Funct. Mater.* **2016**, *26*, 1375–1381. [CrossRef]
90. Zhu, Z.; Hadjiev, V.G.; Rong, Y.; Guo, R.; Cao, B.; Tang, Z.; Qin, F.; Li, Y.; Wang, Y.; Hao, F.; et al. Interaction of organic cation with water molecule in perovskite MAPbI3: From dynamic orientational disorder to hydrogen bonding. *Chem. Mater.* **2016**, *28*, 7385–7393. [CrossRef]
91. Zhou, Y.; Li, C.; Wang, Y.; Du, X.; Liu, P.; Xie, W. Preparation and characterization of high-quality perovskite CH3NH3PbX3 (I, Br) single crystal. In *IOP Conference Series: Materials Science and Engineering*; IOP Publishing: Bristol, UK, 2017.
92. Liu, Y.; Yang, Z.; Cui, D.; Ren, X.; Sun, J.; Liu, X.; Zhang, J.; Wei, Q.; Fan, H.; Yu, F.; et al. Two-inch-sized perovskite CH3NH3PbX3 (X = Cl, Br, I) crystals: Growth and characterization. *Adv. Mater.* **2015**, *27*, 5176–5183. [CrossRef] [PubMed]
93. Liu, Y.; Zhang, Y.; Zhao, K.; Yang, Z.; Feng, J.; Zhang, X.; Wang, K.; Meng, L.; Ye, H.; Liu, M.; et al. A 1300 mm2 ultrahigh-performance digital imaging assembly using high-quality perovskite single crystals. *Adv. Mater.* **2018**, *30*, 1707314. [CrossRef]
94. Fang, H.-H.; Adjokatse, S.; Wei, H.; Yang, J.; Blake, G.R.; Huang, J. Ultrahigh sensitivity of methylammonium lead tribromide perovskite single crystals to environmental gases. *Sci. Adv.* **2016**, *2*, e1600534. [CrossRef]
95. Murali, B.; Dey, S.; Abdelhady, A.L.; Peng, W.; Alarousu, E.; Kirmani, A.R.; Cho, N.; Sarmah, S.P.; Parida, M.R.; Saidaminov, M.I.; et al. Surface restructuring of hybrid perovskite crystals. *ACS Energy Lett.* **2016**, *1*, 1119–1126. [CrossRef]
96. Galisteo-López, J.F.; Calvo, M.E.; Míguez, H. Spatially Resolved Analysis of Defect Annihilation and Recovery Dynamics in Metal Halide Perovskite Single Crystals. *ACS Appl. Energy Mater.* **2019**, *2*, 6967–6972. [CrossRef]
97. Anaya, M.; Galisteo-López, J.F.; Calvo, M.E.; Espinós, J.P.; Míguez, H. Origin of light-induced photophysical effects in organic metal halide perovskites in the presence of oxygen. *J. Phys. Chem. Lett.* **2018**, *9*, 3891–3896. [CrossRef]
98. Ecker, B.R.; Wang, C.; Wei, H.; Yuan, Y.; Huang, J.; Gao, Y. Intrinsic Behavior of CH3NH3PbBr3 Single Crystals under Light Illumination. *Adv. Mater. Interfaces* **2018**, *5*, 1801206. [CrossRef]
99. Syafutra, H.; Yun, J.-H.; Yoshie, Y.; Lyu, M.; Takeda, S.N.; Nakamura, M.; Wang, L.; Jung, M.-C. Surface Degradation Mechanism on CH3NH3PbBr3 Hybrid Perovskite Single Crystal by a Grazing E-Beam Irradiation. *Nanomaterials* **2020**, *10*, 1253. [CrossRef]